Journal of Biomolecular NMR (2021) 75:151–166
https://doi.org/10.1007/s10858-021-00364-y

ARTICLE

Comparative analysis of ^{13}C chemical shifts of β-sheet amyloid proteins and outer membrane proteins

Noah H. Somberg[1] · Martin D. Gelenter[1] · Mei Hong[1]

Received: 8 January 2021 / Accepted: 24 March 2021 / Published online: 12 April 2021

Abstract

Cross-β amyloid fibrils and membrane-bound β-barrels are two important classes of β-sheet proteins. To investigate whether there are systematic differences in the backbone and sidechain conformations of these two families of proteins, here we analyze the ^{13}C chemical shifts of 17 amyloid proteins and 7 β-barrel membrane proteins whose high-resolution structures have been determined by NMR. These 24 proteins contain 373 β-sheet residues in amyloid fibrils and 521 β-sheet residues in β-barrel membrane proteins. The ^{13}C chemical shifts are shown in 2D ^{13}C–^{13}C correlation maps, and the amino acid residues are categorized by two criteria: (1) whether they occur in β-strand segments or in loops and turns; (2) whether they are water-exposed or dry, facing other residues or lipids. We also examine the abundance of each amino acid in amyloid proteins and β-barrels and compare the sidechain rotameric populations. The ^{13}C chemical shifts indicate that hydrophobic methyl-rich residues and aromatic residues exhibit larger static sidechain conformational disorder in amyloid fibrils than in β-barrels. In comparison, hydroxyl- and amide-containing polar residues have more ordered sidechains and more ordered backbones in amyloid fibrils than in β-barrels. These trends can be explained by steric zipper interactions between β-sheet planes in cross-β fibrils, and by the interactions of β-barrel residues with lipid and water in the membrane. These conformational trends should be useful for structural analysis of amyloid fibrils and β-barrels based principally on NMR chemical shifts.

Keywords Chemical shifts · Amyloid proteins · Beta-barrel membrane proteins · Conformational distribution

Introduction

Chemical shifts report the local electronic environment of nuclear spins and are thus sensitive to the conformation and electrostatic interaction of functional groups in molecules. As a result, the different backbone conformations and sidechain structures of amino acids in proteins cause characteristic chemical shift differences. Protein ^{13}C chemical shifts are sensitive to the backbone (ϕ, ψ) torsion angles (Wishart et al. 1991), sidechain χ_1 and χ_2 torsion angles, as well as weak but functionally important interactions such as hydrogen bonding and aromatic interactions (Vranken and Rieping 2009). The empirical relationship between ^{13}C chemical shifts and protein (ϕ, ψ) angles is well established for globular proteins (Wishart and Sykes 1994; Wishart et al. 1991, 1992). By correlating NMR chemical shifts with high-resolution structures solved using distance-restrained NMR data and crystal structures (Shen and Bax 2013; Shen et al. 2009; Spera and Bax 1991), databases such as TALOS-N (Shen and Bax 2013) can predict (ϕ, ψ) and χ_1 angles based on measured Cα, Cβ and CO chemical shifts. While TALOS-N predicts protein torsion angles, the ROSETTA Monte Carlo program has been successfully used to predict the structures of small globular proteins and amyloid proteins based on chemical shifts (Sgourakis et al. 2015; Shen et al. 2008; Skora and Zweckstetter 2012). While structure determination from chemical shifts is the principal goal of NMR spectroscopists, the reverse task of accurately predicting chemical shifts from known structures is also beneficial. This would allow a comparison of protein structures solved using X-ray crystallography and cryoEM with the structures of proteins whose NMR chemical shifts are available. Reliable predictions of chemical shifts can also simplify resonance assignment and facilitate studies of protein dynamics. At present, chemical shifts can be predicted from structures using SHIFTX2 (Han et al. 2011) and SPARTA+ (Shen and

✉ Mei Hong
meihong@mit.edu

[1] Department of Chemistry, Massachusetts Institute of Technology, 170 Albany Street, Cambridge, MA 02139, USA

Bax 2010) software pacakges. But the accuracy of this prediction depends on the extensiveness of the database.

One category of proteins whose structures and chemical shifts became well known in the last decade is the family of cross-β amyloid proteins, whose high-resolution structures were primarily determined using solid-state NMR spectroscopy (Bertini et al. 2011; Colvin et al. 2016; Gelenter et al. 2019; Paravastu et al. 2008; Schütz et al. 2015; Tuttle et al. 2016; Wälti et al. 2016; Xiao et al. 2015). These amyloid proteins are characterized by an X-ray fiber diffraction pattern with a meridian peak corresponding to a distance of ~ 4.8 Å between hydrogen-bonded β-strands and an equatorial peak corresponding to a distance of ~ 10.0 Å between β-sheets. Because these cross-β fibrils have ordered hydrogen bonds across hundreds and thousands of β-strands, we ask the question whether their backbone torsion angles might exhibit systematic differences from β-strands in globular proteins, which are involved in less extensive β-sheets and are not constrained to a two-dimensional plane. If such conformational differences exist, then the chemical shift database established based on globular proteins might not apply well to cross-β amyloid fibrils. In addition to backbone conformation, cross-β amyloid proteins also display distinct sidechain packing from that of globular proteins. Because each hydrogen-bonded β-strand in a cross-β fibril is constrained to a two-dimensional plane containing the fibril axis, the sidechains of one β-sheet can interact with those of an adjacent β-sheet. One well documented sidechain interaction is the steric zipper, defined as interdigitating sidechains between two β-sheets in a dry interior (Nelson et al. 2005; Sawaya et al. 2007). Polar residues such as Gln and Asn are especially capable of forming steric zippers due to their sidechain hydrogen-bonding amide groups. The backbones of two β-strands involved in a steric zipper are ~ 10 Å apart, which is responsible for the equatorial peak in the fiber diffraction patterns. Since solvent exposure can affect NMR chemical shifts (Vranken and Rieping 2009), a dry and interdigitated steric zipper might exhibit distinct sidechain ^{13}C chemical shifts from water-exposed and dynamic β-strand residues in globular proteins.

A second type of β-sheet proteins is the family of β-barrel membrane proteins (Andreas et al. 2016; Hiller et al. 2008; Liang and Tamm 2007; Retel et al. 2017), commonly found in the outer membranes of Gram-negative bacteria. β-barrel proteins contain multiple antiparallel β-strands that traverse the lipid bilayer to enclose a central water-filled pore. Compared to the extended β-sheets of cross-β amyloid fibrils, β-barrels differ in that the hydrogen bonds between neighboring strands are antiparallel rather than parallel; the β-sheet plane has significant curvature in order to bend into the cylindrical barrel surface; and sidechains face either water or lipids, which are highly disordered, instead of other amino acid sidechains. Therefore, β-barrels present an interesting comparison with amyloid proteins for understanding the intrinsic conformational preferences and ^{13}C chemical shifts of β-sheet proteins.

In this work, we analyze the ^{13}C chemical shifts of 17 high-resolution cross-β amyloid protein structures and 7 β-barrel membrane protein structures solved by solid-state and solution NMR, in order to deduce the conformational differences between these two families of proteins. More β-barrel membrane protein structures are available in the literature (Dutta et al. 2017; Horst et al. 2014). However, since a β-barrel protein is typically much larger than an amyloid protein and hence contributes more residues to the dataset, we analyzed a subset of β-barrel structures such that the two datasets have similar numbers of chemical shifts. Two OmpG structures are used: one structure was solved in the detergent octyl-β-glucopyranoside using solution NMR, with only backbone chemical shifts available (Liang and Tamm 2007), while the other structure was solved in *Escherichia coli* lipid extracts using solid-state NMR (Retel et al. 2017) and has both sidechain and backbone chemical shifts. In the amyloid dataset, multiple Aβ40 and Aβ42 structures are used; these Aβ structures are polymorphic and distinct, thus have different chemical shifts. The ^{13}C chemical shifts of these proteins are presented in 2D ^{13}C–^{13}C correlation maps, and the mean and standard deviations of the chemical shifts of each carbon are calculated. We also present the abundance of each amino acid in amyloid proteins, β-barrels and all proteins, and the sidechain χ_1 and χ_2 angle distributions. This analysis allows us to identify several conformational trends that differ between amyloid fibrils and β-barrel membrane proteins for various amino acids.

Methods

The 17 amyloid proteins and 7 β-barrels whose ^{13}C chemical shifts are analyzed here are listed in Table 1. The chemical shifts were obtained from Biological Magnetic Resonance Databank (BMRB) or from the original publications where no BMRB entries are available (Dregni et al. 2019; van der Wel et al. 2007). DSS was used as the chemical shift reference. TMS-referenced chemical shifts were converted to the DSS scale by adding 2.00 ppm to the values (Morcombe and Zilm 2003; Wishart et al. 1995). No change was made to TSP-referenced chemical shifts.

To correlate ^{13}C chemical shifts with structures, we categorized residues according to (1) whether they come from an amyloid protein or a β-barrel protein and (2) whether they lie on a β-strand or in a loop or turn. β-sheet residues in β-barrels are further distinguished by whether they face the lipids or water-filled pore. β-sheet residues in amyloid proteins are further distinguished by whether they face the dry interior or solvent. Non β-strand residues in amyloid proteins

Table 1 Protein structures whose chemical shifts are analyzed in this study

Proteins	Reference	pH	T (K)	BMRB #	PDB #	CS reference	Strand[a]	No. β-sheet residues[b]	Total no. residues[c]
Aβ40	Lu et al. (2013)	7.4	273	19009	2M4J	DSS	D	22	38
Aβ40	Bertini et al. (2011)	8.5	283	34454	6TI5	TSP	C	22	30
Aβ40	Paravastu et al. (2008)	7.4	300	18131	2LMQ	TMS	C	12	32
Osaka Aβ40	Schütz et al. (2015)	7	273	25289	2MVX	DSS	D	19	37
Aβ42	Colvin et al. (2016)	8	277	30121	5KK3	DSS	D	13	30
Aβ42	Wälti et al. (2016)	7.4	273	26692	2NAO	DSS	E	18	40
Aβ42	Gremer et al. (2017)	2	278	27212	5OQV	DSS	C	30	42
α-synuclein	Tuttle et al. (2016)	7	273	25518	2N0A	DSS	E	48	138
HET-s	Wasmer et al. (2008)	7.5	278	11028	2RNM	DSS	C	28	77
Necrosome	Mompeán et al. (2018)	6.5	278	30273	5V7Z	DSS	D, E	20	33
FUS-LC	Murray et al. (2017)	7.4	298	30304	5W3N	DSS	E	20	59
Tau[d]	Dregni et al. (2019)	7.4	260–293	–	–	TMS	N/A	30	30
Glucagon	Gelenter et al. (2019)	2.0	293	30572	6NZN	TMS	E, K	51	54
GNNQQNY[e]	Sawaya et al. (2007), van der Wel et al. (2007)	2–3	277	–	2OMM	DSS	A	7	7
TTR	Fitzpatrick et al. (2013)	2	298	19062	2M5N	DSS	D	11	11
Zn-binding fibril	Lee et al. (2017)	8	298	30227	5UGK	TMS	D	5	5
MAX1	Nagy-Smith et al. (2015)	9	273	25558	2N1E	DSS	C	17	20
							Total	373	683
VDAC-1	Hiller et al. (2008)	7.0	303	16381	2K4T	DSS	N/A	169	283
OmpA BBP	Johansson et al. (2007)	6	303	15045	2JMM	DSS	N/A	84	156
OmpG	Liang and Tamm (2007)	6.3	313	15426	2JQY	DSS	N/A	178	275
OmpG	Retel et al. (2017)	6.8	280	34088	5MWV	DSS	N/A	121	279
OmpX	Hagn et al. (2013)	6.5	318	18796	2M06	DSS	N/A	100	148
OprH	Edrington et al. (2011)	6.1	273	17842	2LHF	DSS	N/A	79	178
YadA	Shahid et al. (2012)	7	275	18108	2LME	DSS	B	43	105
							Total	521	985

[a]An interior β-strand in the deposited amyloid protein structure that is selected to extract torsion angles

[b]The number of residues in the β-sheet conformation

[c]The total number of residues in one β-strand for amyloid fibrils and the total number of residues in the β-barrel structures

[d]Chemical shifts were extracted directly from the publication. No BMRB or PDB entry exists for this publication, and no secondary structural data was used

[e]Secondary structural data was extracted from PDB entry 2OMM (Sawaya et al. 2007). Chemical shifts were extracted directly from (van der Wel et al. 2007) No BMRB entry exists for this publication

are also distinguished by whether they are dry or solvent-exposed. In β-barrels, non β-sheet residues often cannot be clearly distinguished between water-exposed and lipid-exposed positions, thus we did not make further distinctions for loop, turn, or helical residues in β-barrels. In total, six structural categories were created for each amino acid: water-exposed β-sheet residues in β-barrels, lipid-exposed β-sheet residues in β-barrels, dry β-sheet residues in fibrils, water-exposed β-sheet residues in fibrils, dry loop or turn residues in fibrils, and water-exposed loop or turn residues in fibrils (Table 2). We compiled and analyzed the chemical shifts of the six categories, excluding the non-β-sheet residues in β-barrels. The average and standard deviation of β-sheet residues in fibrils and β-barrels are tabulated in Table 3.

Conformational information, including (ϕ, ψ) and (χ_1, χ_2) torsion angles and the β-sheet designations, was obtained from the Protein Data Bank (PDB). For structures without PDB entries, information such as β-sheet designation and sidechain structure were obtained from the original publication. For PDB entries that include multiple copies of the same β-strand, we extracted a single monomer from the center of the deposited structure to avoid potential torsion angle distortions due to edge defects. For protein structures that have multiple conformations, we analyzed the lowest energy conformation.

Table 2 Number of residues in six structural categories used for the chemical shift analysis

Residues	All proteins			β-barrel β-sheets		Cross-β fibrils			
	Total	Barrel	Fibril	Lipid facing	Water-facing	β-sheet, dry	β-sheet, wet	Loop/turn, dry	Loop/turn, wet
ALA	147	99	48	34	29	15	5	9	19
ARG	80	66	14	3	31	4	6	1	3
ASN	126	98	28	7	30	8	5	8	7
ASP	133	101	32	6	17	6	6	4	16
CYS	3	2	1	1	1	1	0	0	0
GLN	93	53	40	17	17	13	11	9	7
GLU	123	82	41	5	32	3	11	3	24
GLY	250	163	87	24	74	11	11	11	54
HIS	49	22	27	3	4	6	7	2	12
ILE	80	45	35	28	3	22	3	3	7
LEU	140	110	30	58	10	17	4	4	5
LYS	112	66	46	7	24	2	24	1	19
MET	35	22	13	5	8	3	4	2	4
PHE	96	71	25	40	9	8	7	6	4
PRO	46	37	9	10	1	2	0	0	7
SER	146	92	54	7	35	12	11	15	16
THR	124	94	30	16	32	9	9	7	5
TRP	38	35	3	17	3	0	2	0	1
TYR	126	96	30	51	26	6	8	3	13
VAL	159	70	89	39	10	37	23	17	12
Total	2106	1424	682	378	396	185	157	105	235

All torsion angles were analyzed in PyMol. Sidechain torsion angles were obtained using a home-written PyMol script that measures each angle from the PDB structure. For structures with multiple identical subunits, we chose a single subunit from the interior of the structure. For the χ_1 angle around the Cα–Cβ bond, 0° is defined as when the Cβ–Cγ bond is aligned with the N-Cα bond. For the χ_2 angle around the Cβ–Cγ bond, 0° is defined as when the Cα–Cβ bond is aligned with the Cγ–Cδ bond. (Lovell et al. 2000).

Home-written MATLAB scripts were used to extract the chemical shifts of each amino acid residue and to associate the chemical shifts with the structural categories. This dataset was used to construct the 2D ^{13}C–^{13}C chemical shift maps for each amino acid type. A given ^{13}C chemical shift was correlated to all other chemical shifts in the same residue, thus the constructed 2D correlation map represent all possible combination of ^{13}C–^{13}C cross peaks within a residue.

For a given cross peak such as Cα–Cβ in one of the six structural categories, the mean of the chemical shifts for β-sheet residues was computed for both the direct and indirect dimensions. An ellipse was then plotted with its center at the position of the mean in each dimension. The standard deviation of the β-sheet chemical shifts is calculated for each dimension and represented as half the semi-major and semi-minor axes lengths of the ellipse. In other words, the ellipse represents twice the standard deviation of the chemical shift in each dimension. These ellipses are plotted separately for fibril and barrel β-sheet residues, and separately for each type of cross peaks for a given amino acid. The ellipse positions and sizes are calculated using a MATLAB script that computes the mean and 2σ confidence interval for each cross peak. The chemical shift limits for each type of cross peaks are defined manually. When the boundary of a cross peak crosses the diagonal, we only calculated the chemical shifts of peaks on one side of the diagonal.

Results and discussion

We first examined the abundance of each amino acid in the β-sheet segments of amyloid fibrils, β-barrels, and all proteins in the UniProtKB/Swiss-Prot databank (Consortium 2018). The percentages are relative to the total number of residues in each of the three protein categories. Figure 1 shows that Val is highly enriched in amyloid proteins, accounting for more than 1/6 of all residues. This is consistent with the known ability of the two methyl groups of the Val sidechain to engage in steric zipper interactions (Nelson et al. 2005). Ile and Gln are also enriched in amyloid proteins relative to their abundance in all proteins. In comparison, several amino acids such as Arg and Leu are

Table 3 Mean and standard deviation of ^{13}C chemical shifts for β-sheet residues in cross-β fibrils and β-barrels. Trp and Cys are omitted due to insufficient statistics

Residue	Atom	Average chemical shift of β-sheet residues			BMRB average CS (Ulrich et al. 2008)	Count	
		Fibrils	Barrels	ΔCS		Fibrils	Barrels
Ala	C	175.6 ± 1.7	175.5 ± 0.9	0.0	177.8	18	46
	CA	50.5 ± 0.4	50.6 ± 1.0	− 0.2	53.2	18	59
	CB	21.9 ± 2.2	22.8 ± 1.4	− 0 .9	19.0	18	56
Arg	C	174.6 ± 0.9	174.2 ± 0.9	0.4	176.5	8	28
	CA	54.8 ± 0.3	54.5 ± 0.9	0.3	56.8	8	30
	CB	33.9 ± 0.9	33.8 ± 2.2	0.1	30.6	8	30
	CD	43.5 ± 1.0	44.3 ± 0.4	− 0.8	43.2	7	8
	CG	27.4 ± 0.7	27.4 ± 0.9	0.1	27.2	7	8
	CZ	159.7 ± 0.4	159.6 ± 0.2	0.1	159.9	4	9
Asn	C	174.4 ± 1.6	173.6 ± 1.2	0.8	175.3	11	25
	CA	53.1 ± 1.0	52.4 ± 1.1	0.8	53.5	12	35
	CB	41.1 ± 2.9	41.8 ± 2.0	− 0.8	38.7	11	35
	CG	176.3 ± 1.1	177.7 ± 0.7	− 1.5	176.7	10	4
Asp	C	173.8 ± 0.5	174.4 ± 1.3	− 0.6	176.4	9	13
	CA	52.7 ± 0.8	53.3 ± 1.0	− 0.5	54.7	9	20
	CB	41.6 ± 2.7	43.3 ± 1.6	− 1.7	40.9	9	21
	CG	178.7 ± 1.7	180.3 ± 0.7	− 1.7	178.9	9	2
Gln	C	174.1 ± 1.0	174.3 ± 1.3	− 0.2	176.4	18	24
	CA	54.3 ± 0.9	54.1 ± 1.1	0.2	56.6	19	31
	CB	32.9 ± 1.1	31.7 ± 2.4	1.2	29.2	19	30
	CD	178.6 ± 1.6	179.9 ± 0.3	− 1.3	179.7	16	2
	CG	33.8 ± 1.5	35.0 ± 1.7	− 1.2	33.8	14	3
Glu	C	174.0 ± 1.1	174.6 ± 1.2	− 0.6	176.9	10	22
	CA	54.6 ± 1.7	54.9 ± 1.2	− 0.3	57.3	12	31
	CB	32.6 ± 1.3	32.8 ± 2.2	− 0.3	30.0	12	27
	CD	182.5 ± 0.9	183.2 ± 0.8	− 0.7	182.3	8	3
	CG	36.5 ± 1.6	37.4 ± 0.5	− 0.9	36.1	9	4
Gly	C	171.5 ± 1.6	171.2 ± 1.2	0.2	173.9	18	72
	CA	45.9 ± 2.0	45.3 ± 1.0	0.7	45.4	19	89
His	C	173.4 ± 0.7	173.6 ± 1.6	− 0.2	175.3	12	5
	CA	52.0 ± 1.4	55.0 ± 0.7	− 3.1	56.5	11	6
	CB	32.8 ± 1.5	32.0 ± 1.7	0.9	30.3	11	6
	CD2	117.4 ± 3.4	121.3 ± 0.7	− 3.9	120.3	10	3
	CE1	139.8 ± 5.0	136.8 ± 1.3	2.9	137.6	7	2
	CG	134.6 ± 2.8	133.2 ± 3.6	1.4	132.2	10	3
Ile	C	174.5 ± 1.1	173.8 ± 1.4	0.7	176.0	23	19
	CA	59.6 ± 1.1	59.6 ± 1.3	0.0	61.7	25	29
	CB	40.8 ± 1.8	41.0 ± 1.8	− 0.3	38.6	24	27
	CD1	14.1 ± 1.0	14.5 ± 0.8	− 0.3	13.4	21	14
	CG1	27.4 ± 0.6	28.3 ± 1.1	− 1.0	27.7	20	6
	CG2	17.8 ± 0.8	18.7 ± 0.6	− 0.9	17.5	22	6
Leu	C	174.9 ± 1.5	175.0 ± 1.3	− 0.1	177.1	17	41
	CA	54.3 ± 1.3	53.5 ± 0.9	0.8	55.7	18	66
	CB	44.5 ± 1.6	45.7 ± 1.8	− 1.1	42.2	17	61
	CD1	25.1 ± 1.8	25.1 ± 1.0	0.1	24.6	16	33
	CD2	24.9 ± 2.6	25.4 ± 1.0	− 0.5	24.1	14	26
	CG	28.5 ± 1.4	28.1 ± 0.7	0.4	26.8	15	12

Table 3 (continued)

Residue	Atom	Average chemical shift of β-sheet residues			BMRB average CS (Ulrich et al. 2008)	Count	
		Fibrils	Barrels	ΔCS		Fibrils	Barrels
Lys	C	174.0 ± 1.2	174.8 ± 1.1	− 0.8	176.7	13	15
	CA	55.4 ± 1.5	54.8 ± 1.1	0.6	57.0	13	30
	CB	36.2 ± 1.8	35.4 ± 1.8	0.8	32.8	12	26
	CD	30.0 ± 0.8	30.2 ± 1.5	− 0.1	29.0	8	4
	CE	42.1 ± 0.4	42.1 ± 0.6	− 0.1	41.9	7	4
	CG	25.7 ± 0.4	24.2 ± 1.9	1.6	24.9	10	4
Met	C	173.9 ± 0.8	174.2 ± 0.8	− 0.3	176.3	6	8
	CA	54.2 ± 1.4	54.0 ± 0.7	0.2	56.2	6	13
	CB	36.9 ± 1.1	36.4 ± 1.3	0.5	32.9	6	12
	CE	17.5 ± 0.6	16.8 ± 1.7	0.7	17.1	5	4
	CG	32.1 ± 0.6	32.6 ± 0.8	− 0.5	32.0	5	4
Phe	C	173.7 ± 1.1	173.9 ± 1.6	− 0.2	175.5	13	28
	CA	55.4 ± 2.3	56.6 ± 1.9	− 1.2	58.1	13	44
	CB	42.8 ± 1.7	42.2 ± 1.7	0.7	39.9	13	40
	CD1	130.8 ± 1.1	132.2 ± 0.3	− 1.4	131.6	6	2
	CD2	131.6 ± 0.9	132.2 ± 0.3	− 0.6	131.6	6	2
	CE1	131.4 ± 0.6	130.2 ± 1.7	1.1	130.7	4	3
	CE2	131.6 ± 0.8	130.2 ± 1.7	1.4	130.7	2	3
	CG	139.2 ± 2.0	139.5 ± 0.5	− 0.4	138.3	9	9
	CZ	129.1 ± 1.1	129.1	0.0	129.2	4	1
Pro	C	175.7 ± 1.3	175.8 ± 1.0	− 0.1	176.8	2	9
	CA	62.5 ± 0.2	62.6 ± 0.7	− 0.2	63.4	2	10
	CB	32.5 ± 0.2	33.5 ± 0.7	− 1.0	31.8	2	10
	CD	48.4 ± 1.7	50.7 ± 0.9	− 2.3	50.3	2	4
	CG	28.3 ± 0.4	28.0 ± 0.6	0.2	27.2	2	4
Ser	C	173.6 ± 2.4	172.9 ± 0.9	0.8	174.6	17	27
	CA	56.8 ± 1.3	57.0 ± 0.8	− 0.3	58.7	15	41
	CB	65.6 ± 1.4	65.7 ± 1.3	− 0.2	63.8	16	40
Thr	C	173.5 ± 1.3	172.5 ± 1.5	1.0	174.6	15	26
	CA	61.0 ± 1.0	60.3 ± 1.3	0.7	62.2	16	45
	CB	71.2 ± 1.2	70.9 ± 1.1	0.3	69.7	15	42
	CG2	21.6 ± 1.1	21.0 ± 2.0	0.6	21.5	14	7
Tyr	C	175.5 ± 3.2	173.6 ± 1.3	1.9	175.5	10	52
	CA	57.1 ± 1.6	56.5 ± 1.2	0.6	58.2	10	71
	CB	40.7 ± 2.1	41.8 ± 1.2	− 1.1	39.3	10	71
	CD1	133.1 ± 0.8	132.7 ± 0.5	0.3	132.7	7	5
	CD2	133.2 ± 0.5	132.7 ± 0.5	0.5	132.7	7	5
	CE1	118.1 ± 0.5	117.9 ± 0.4	0.2	117.9	9	6
	CE2	117.9 ± 0.4	117.9 ± 0.4	− 0.1	117.9	6	6
	CG	128.8 ± 2.0	130.3 ± 1.6	− 1.4	129.7	9	12
	CZ	157.5 ± 1.1	158.8 ± 0.6	− 1.3	156.7	8	4
Val	C	174.4 ± 1.6	173.8 ± 1.2	0.6	175.7	43	38
	CA	60.5 ± 1.1	60.2 ± 1.6	0.4	62.6	45	47
	CB	34.9 ± 1.4	34.9 ± 1.3	0.0	32.7	44	46
	CG1	21.4 ± 0.9	21.2 ± 1.2	0.1	21.5	40	15
	CG2	20.8 ± 1.3	21.6 ± 0.5	− 0.8	21.3	34	11

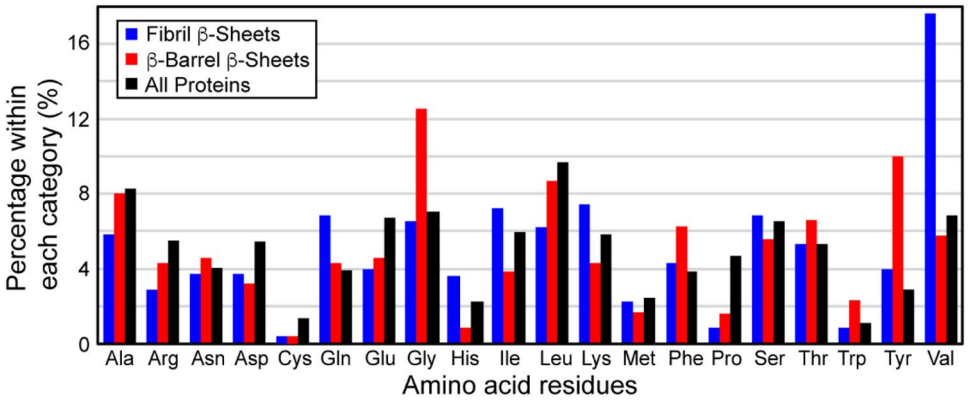

Fig. 1 Percentages of each amino acid residue in three structural categories: all proteins in the UniProtKB/Swiss-Prot databank (black); β-sheet segments of amyloid proteins analyzed here (blue); and β-sheet segments of β-barrel membrane proteins analyzed here (red). Val, Gln, Ile and Lys are over-represented in amyloid fibril β-sheets relative to β-barrel membrane proteins and all proteins. In comparison, Gly and Tyr are over-represented in β-barrel membrane proteins relative to amyloid fibrils as well as all proteins

depleted in cross-β fibrils, suggesting steric and electrostatic effects. In β-barrel membrane proteins, Val is less enriched relative to their abundance in all proteins, while Gly, Tyr and Phe are over-represented relative to their abundance in all proteins. These statistics suggest that the structural flexibility of Gly and the aromatic interactions of Tyr and Phe with lipids may be important for stabilizing β-barrels in lipid bilayers.

We analyzed 17 amyloid fibrils and 7 β-barrel structures for which high-resolution structures and chemical shift data are available (Table 1). These amyloid proteins and β-barrels contain 683 and 985 residues, respectively, among which 373 (55%) residues in fibrils and 521 (53%) residues in β-barrels are located in β-strands. The remaining residues lie in loops, turns, or short helices. All residues are used for parsing the (φ, ψ) torsion angles and (χ_1, χ_2) rotameric angles, but only residues with reported chemical shifts can be used for constructing the 2D ^{13}C–^{13}C correlation maps. To illustrate the structural categories analyzed here, Fig. 2 depicts the structures of three amyloid proteins, Aβ42, Osaka Aβ40, and glucagon; and two β-barrels, VDAC-1 and OmpG. Glucagon is an example of a long and straight antiparallel hydrogen-bonded β-strand with alternating dry steric-zipper residues and water-exposed residues (Fig. 2a). Aβ42 and Osaka Aβ40 form parallel-in-register β-sheets where the two protofibrils contain β-strands interspersed by disordered turns (Fig. 2b, c). VDAC-1 and OmpG are two β-barrel proteins containing 19 and 14 β-strands, respectively. Each β-strand has a pore-facing side and a lipid-facing side (Fig. 2e), which are preferentially enriched in polar and hydrophobic residues, respectively. Table 2 lists the number of each amino acid in the chemical shift dataset, broken down according to the six structural categories. The percentages of residues in each structural environment for Val, Leu, Gly, Ala, Gln, and Arg are also shown in Fig. 3.

We present the ^{13}C chemical shifts in 2D ^{13}C–^{13}C correlation maps for thirteen amino acids. These amino acids are chosen for their high abundance in these β-sheet proteins, with either at least 50 occurrences in the combined dataset or with a high prevalence among either amyloid fibrils or β-barrel β-sheets. In our analysis, we consider chemical shift differences of 0.5 ppm or larger to be significant based on the typical ^{13}C linewidths of solid-state proteins. Figure 4 shows the 2D ^{13}C–^{13}C correlation map of Val. Val exhibits a narrower Cα chemical shift distribution but a larger Cγ chemical shift distribution in amyloid fibrils compared to β-barrels (Fig. 4b). The Cα chemical shift standard deviation ($\sigma_{C\alpha}$) is 1.1 ppm in fibrils and increases to 1.6 ppm in β-barrels (Table 3), suggesting that the extended hydrogen-bonding in cross-β fibrils narrows the Val backbone conformational distribution compared to β-barrel Val residues. In contrast, the Val Cγ2 chemical shift distribution is much wider (1.3 ppm) in cross-β fibrils than in β-barrels (0.5 ppm). The former is mostly contributed by dry β-sheet residues, suggesting that the participation of Val in steric zippers in amyloid fibrils increases the static conformational disorder of the sidechain.

Figure 5 displays the 2D ^{13}C–^{13}C chemical shift correlation maps of the two other methyl-rich hydrophobic residues, Leu and Ile. In contrast to Val, Leu shows much larger Cα, Cγ and Cδ chemical shift dispersions in amyloid fibrils than in β-barrels. The difference is mainly manifested by dry fibril residues and lipid-facing residues in β-barrels. This observation suggests that water exposure in either protein leads to similar averaged sidechain conformations, whereas the dry fibril interior, including steric zippers, creates larger static conformational disorder compared to lipid-facing residues. For Ile, the Cγ1 methyl chemical shift is more narrowly distributed in fibrils (0.6 ppm) than in β-barrels (1.1 ppm) (Fig. 5b), and the Cγ1 and Cγ2 chemical shifts are 0.9–1.0 ppm shifted upfield in amyloid fibrils than in

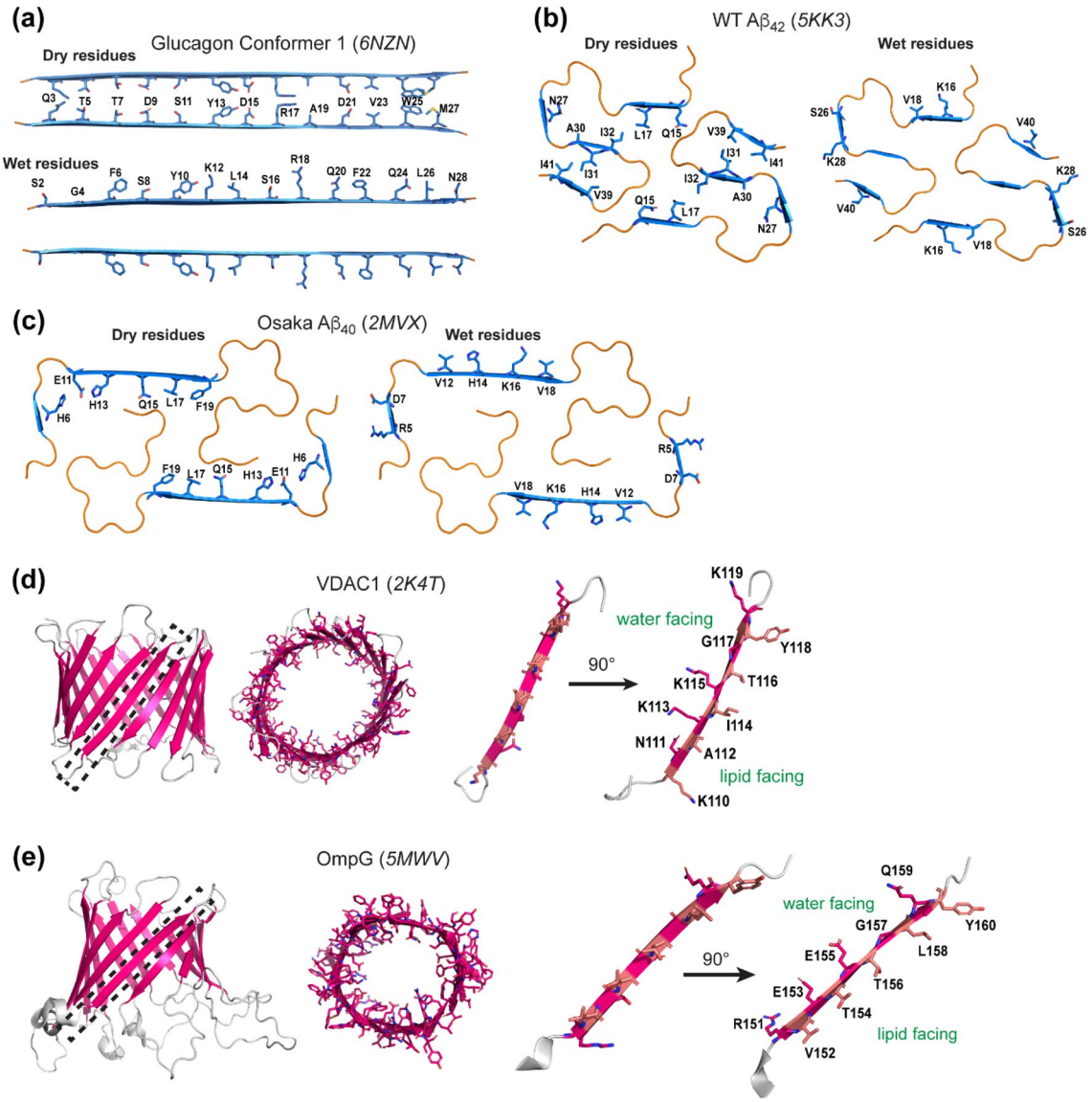

Fig. 2 Representative structures of amyloid fibrils and β-barrels (with PDB accession codes in brackets) analyzed in this study and the categories of amino acid residues whose chemical shifts are evaluated. **a–c** Representative amyloid protein structures. β-sheet backbones are depicted in blue and loops are shown in orange. **a** Conformer 1 of the dimeric glucagon fibril (PDB: 6NZN). Dry residues lining the dimer interface (*top*) and solvent-exposed wet residues (*bottom*) are shown separately. **b** Wild-type $A\beta_{42}$ fibrils (PDB: 5KK3). Interior-facing dry residues and exterior-facing water-exposed residues are shown separately. **c** Osaka mutant Aβ40 fibrils (PDB: 2MVX). **d** Membrane-bound structure of the β-barrel VDAC1 (PDB: 2K4T). **e** Membrane-bound structure of the β-barrel OmpG (PDB: 5MWV). For **d**, **e**, β-sheet backbones are shown in magenta, whereas α-helical and loop residues are shown in gray. Water-facing and lipid-facing sidechains of representative β-strands are shown

β-barrels (Table 3). Thus, sidechain conformational differences exist between the two types of proteins, which may be caused by sidechain packing in cross-β amyloid fibrils versus protein-lipid interactions in β-barrels.

The ^{13}C chemical shift distributions of the small Gly and Ala residues also differ between amyloid fibrils and β-barrels (Fig. 6), with fibrils exhibiting larger chemical shift dispersion than β-barrels. Gly residues in both the β-strand and turn regions of fibrils contribute to the Cα and CO chemical shift dispersion, whereas the β-barrel Gly Cα and CO chemical shifts are tightly clustered, especially for water-facing Gly residues (Fig. 6a). These trends indicate that the amphipathic β-strands in β-barrels, sandwiched by lipids on one side and a water-filled pore on the other, constrain the backbone conformation of Gly more than the cross-β fibril. Indeed, Gly in amyloid fibrils predominantly appear in flexible loop regions (Fig. 3c), whereas in β-barrels more than half of the Gly residues are located in β-sheet segments.

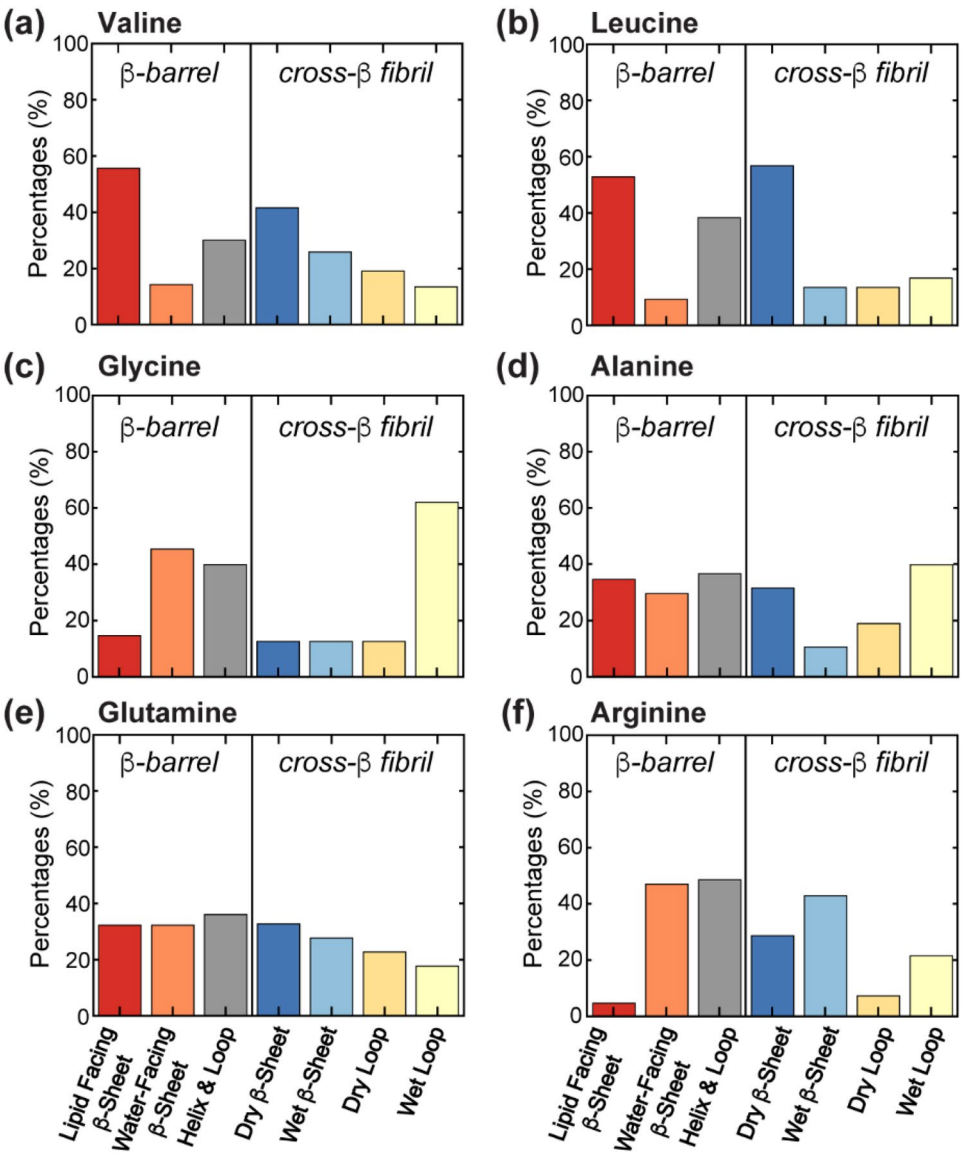

Fig. 3 Percentages of an amino acid in a certain structural environment of β-barrels and amyloid fibrils for six amino acids. β-barrel residues are categorized into lipid-facing β-sheet residues, water-facing β-sheet residues, and all other residues. Cross-β fibril residues are categorized into dry β-sheet residues, wet β-sheet residues, dry loop residues, and wet loop residues. **a** Valine distribution. Val residues in β-barrels are enriched in lipid-facing β-sheets. **b** Leucine distribution. Leu residues in β-barrels are enriched in lipid-facing β-sheets whereas Leu in amyloid fibrils are enriched in dry β-sheets. **c** Glycine distribution. Gly residues in amyloid fibrils are mostly located in wet loop segments. **d** Alanine distribution. **e** Glutamine distribution. **f** Arginine distribution. Arg residues in β-barrels are mostly excluded from lipid-facing β-sheet segments

This could be due to the unusually long β-strands found in β-barrels, which cause backbone conformational strains that is alleviated by the flexible Gly residues. Ala also exhibits larger chemical shift dispersions for all carbons in fibrils than in membrane-bound β-barrels (Fig. 6b). For Ala Cβ, even when chemical shifts from turn residues are excluded, the majority of the β-sheet residues in fibrils display a larger chemical shift dispersion than in β-barrels.

Compared to the small Gly and Ala, the bulky aromatic Phe exhibits distinct chemical shifts between the cross-β fibrils and membrane-bound β-barrels. Among the sidechain carbons, Phe Cγ chemical shift is significantly more distributed in fibrils than in barrels, with a standard deviation of 2.0 ppm in fibrils and 0.5 ppm in β-barrels (Table 3). These differences indicate that the Phe sidechain conformation, dictated by the χ_1 torsion angle, has a larger static disorder in amyloid fibrils, which is likely caused by aromatic stacking in the dry steric zipper interface. In comparison, Phe sidechains in membrane-bound β-barrels may undergo significant conformational motion, thus giving narrowly clustered aromatic ^{13}C chemical shifts.

Figure 7 compares the ^{13}C chemical shift correlation maps of six polar residues, including Glu, Gln, Asn, Ser, Thr and Tyr. Glu ^{13}C chemical shifts do not display significant differences between fibrils and barrels. In contrast, the Gln Cβ chemical shifts are much more narrowly distributed in amyloid fibrils than in barrels, as shown by the Cβ–Cγ and Cα–Cγ correlation peaks: the $\sigma_{C\beta}$ value is 1.1 ppm for fibril Gln residues and increases to 2.4 ppm for β-barrel Gln residues (Table 3, Fig. 7b). Moreover, the mean Cβ, Cγ and Cδ chemical shifts deviate by ~ 1.2 ppm between fibril and barrel Gln residues. Gln residues play a key role

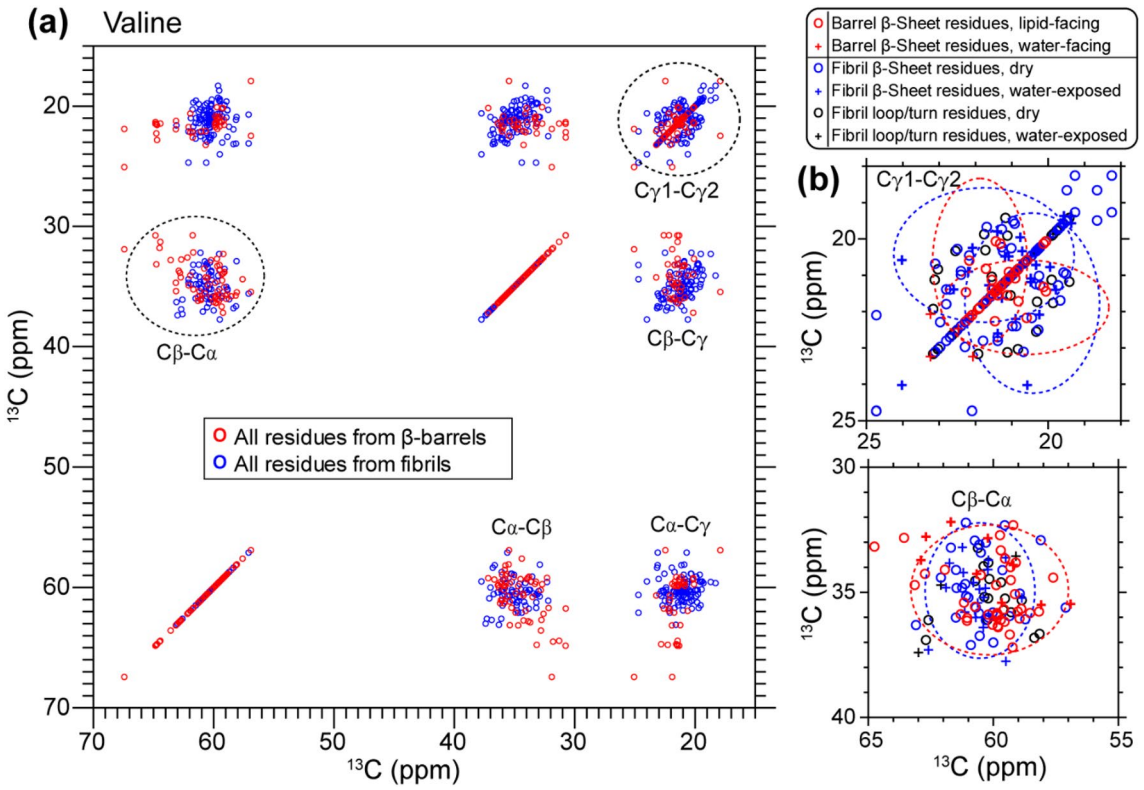

Fig. 4 2D ^{13}C–^{13}C correlation map of valine. **a** Full aliphatic region, showing β-barrel cross peaks in red and amyloid fibril cross peaks in blue. **b** Zoomed-in Cγ methyl ^{13}C chemical shift region and Cβ–Cα cross peak region. Residues are sorted into six categories as indicated in the upper right corner. Dashed lines denote the 2σ boundary from the mean of the β-barrel β-sheet chemical shifts (red) and the fibril β-sheet chemical shifts (blue). Chemical shift axes are in ppm from DSS

in steric zippers due to the hydrogen-bonding ability of the amide sidechain, which stabilizes the β-strand interface. Canonical steric zippers such as GNNQQNY in the yeast prior protein Sup35, and VQIINK and VQIVYK in the tau protein, all contain Gln residues (Nelson et al. 2005; Sawaya et al. 2007). Thus, the narrow Cβ chemical shift distribution of Gln in fibrils suggests preferential rotameric conformation and/or hydrogen-bonding of the Gln sidechain. This sidechain order differs from the sidechain disorder of Val, although both amino acids are common in steric zippers of amyloid proteins. We examined the (χ_1, χ_2) torsion angle distributions of the amino acids in cross-β fibrils and β-barrels (Fig. 9) and did not find the Gln and Val rotamer distributions to be narrower in fibrils than in β-barrels. Thus, we attribute the narrow chemical shift distribution of Gln residues in amyloid fibrils to sidechain hydrogen bonding in steric zippers, while the larger Val chemical shift dispersion is attributed to the χ_1 torsional angle distribution. Interestingly, Asn, which also possesses an amide sidechain but is one CH_2 group shorter than Gln, and which also occurs frequently in steric zippers, exhibits a larger Cβ chemical shift distribution in fibrils ($\sigma_{C\beta}$ = 2.9 ppm) than in β-barrels ($\sigma_{C\beta}$ = 2.0 ppm) (Fig. 7c, Table 3). These chemical shift dispersions are mainly contributed by water-exposed Asn residues, suggesting that the shorter sidechain endows Asn with larger conformational freedom compared to Gln residues.

The hydroxy-bearing Ser and Thr residues exhibit different Cα chemical shift trends: the Ser Cα chemical shift is more distributed in amyloid fibrils than β-barrel membrane proteins, as seen in the Cβ–Cα correlation peaks (Fig. 7d), whereas Thr Cα and Cγ chemical shifts are more narrowly clustered in amyloid fibrils than in β-barrels (Fig. 7e). For the hydroxy-bearing aromatic Tyr, most ^{13}C chemical shifts are more distributed in amyloid fibrils than in β-barrels (Fig. 7f). Interestingly, the average Tyr Cβ chemical shifts differ noticeably between fibrils and barrels: the former is 1.1 ppm smaller than the latter (Table 3, Fig. 7f). The Tyr χ_1 angles are similarly distributed in fibrils and barrels: both proteins exhibit a preference for the *trans* (180°) and -60° states over the + 60° state (Fig. 8). Thus, at present we attribute this Cβ chemical shift difference to small backbone conformational differences between amyloid fibril Tyr residues and β-barrel Tyr residues.

The 2D ^{13}C–^{13}C correlation map of the cationic Arg shows an interesting trend where most carbons except for Cδ

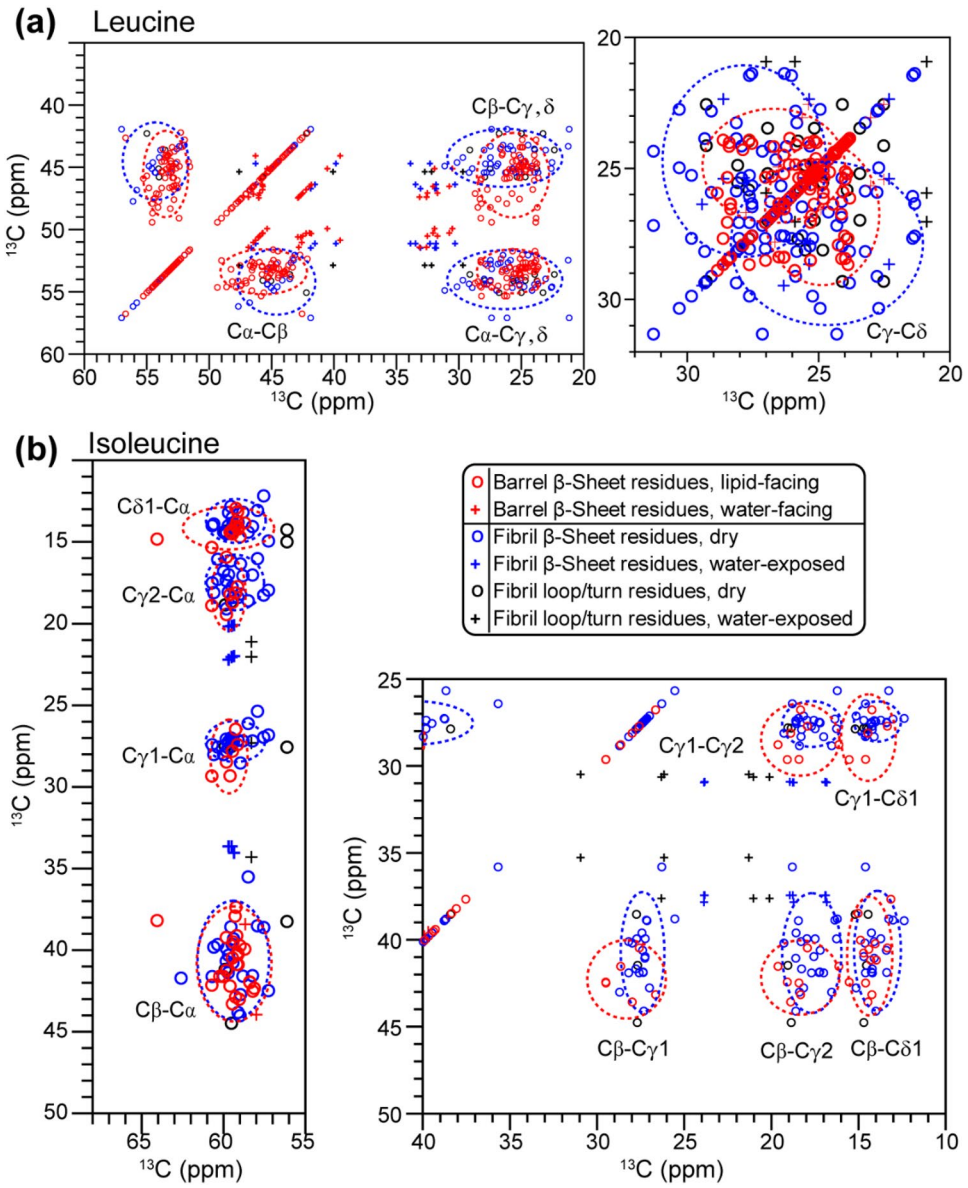

Fig. 5 Selected regions of the 2D ^{13}C–^{13}C correlation maps of two hydrophobic residues. **a** Leucine. **b** Isoleucine. Symbol keys are the same as in Fig. 4. Dashed lines denote the 2σ boundary from the mean of the β-sheet chemical shifts in β-barrels (red) and fibrils (blue). Ile exhibits smaller (upfield) Cβ chemical shifts and a narrower Cγ1 chemical shift distribution in fibrils than in β-barrels. In contrast, Leu methyl ^{13}C chemical shifts have the opposite trend of being much more widely distributed in fibrils than in β-barrels

and Cζ have narrower chemical shift distributions in amyloid fibrils than in β-barrels (Fig. 9). We attribute the backbone conformational order of Arg in cross-β fibrils to the constraints of extensive β-strand hydrogen bonds, while the relative disorder of Arg in membrane proteins is attributed to the high energetic cost of inserting Arg into the hydrophobic portion of lipid bilayers (Moon and Fleming 2011). In comparison, the Arg guanidinium group can form bidentate complexes with lipid phosphate groups, stabilized by electrostatic attraction and hydrogen bonding. This salt bridge interaction is well documented for Arg-rich antimicrobial peptides based on distance measurements between Arg Cζ and lipid ^{31}P (Su et al. 2009; Tang et al. 2007). This salt bridge interaction should narrow the conformational distribution of the end of the Arg sidechain in the lipid membrane, thus explaining the narrow Cδ and Cζ chemical shift distribution in β-barrels.

We summarize the ^{13}C chemical shifts and the ensuing conformational trends of these 13 amino acids in β-sheet proteins as follows. Specifically, we focus on the static conformational disorder, which is reflected by chemical shift distributions. First, bulky methyl-rich hydrophobic residues (Val, Leu and Ile) exhibit more ordered backbone but more disordered sidechain conformations in cross-β fibrils than in β-barrels. This sidechain disorder is static in nature, manifested as larger chemical shift distributions in fibrous residues. Second, the small Ala and Gly are more disordered in fibrils than in barrels. Third, aromatic Phe and Tyr residues have more disordered backbone and sidechain conformations in amyloid fibrils than in β-barrels. Fourth, the polar

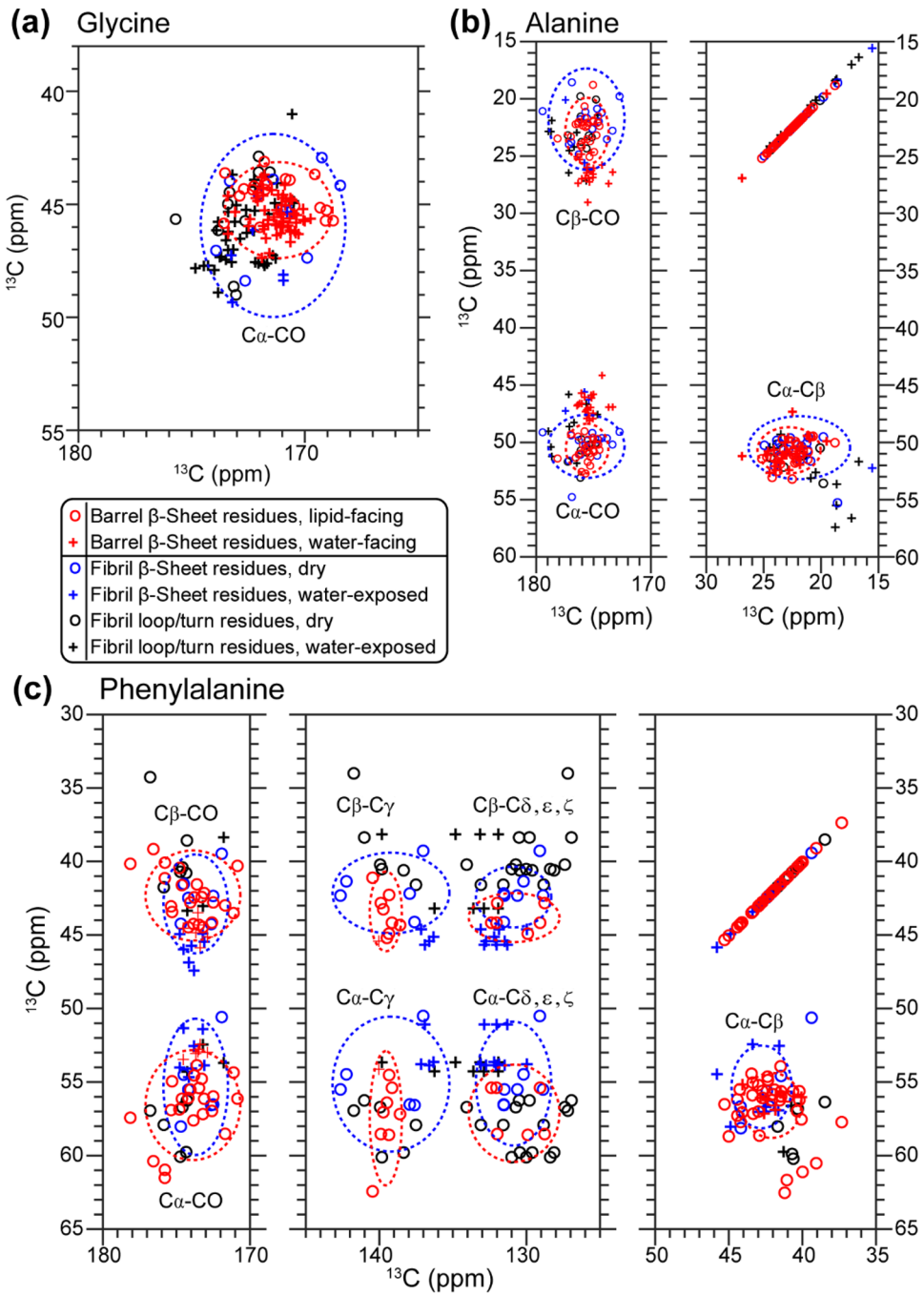

Fig. 6 Selected regions of the 2D ^{13}C–^{13}C correlation maps of **a** glycine, **b** alanine, and **c** phenylalanine. Symbol keys are the same as in Fig. 4. Both Gly and Ala show larger ^{13}C chemical shift distributions for all carbons in amyloid fibrils than in β-barrels. Phe has a narrower CO chemical shift distribution but wider Cγ chemical shift distribution in fibrils than in β-barrels

Ser, Thr and Arg are more structurally ordered in fibrils than in barrels. Finally, Gln and Asn exhibit opposite sidechain conformational trends: Gln is more ordered in fibrils than β-barrels, whereas Asn is more disordered in amyloid fibrils.

One of the clearest chemical shift differences between amyloid fibrils and β-barrels is found for Val and Leu methyl carbons (Figs. 4, 5): fibrous Val and Leu residues, particularly those located at the dry β-strand interface, display much larger methyl ^{13}C chemical shift distributions than β-barrel Val and Leu residues. Recent studies of several amyloid proteins, including glucagon and the tau protein (Dregni et al. 2019; Gelenter et al. 2019), reported a splitting in the Val methyl groups that are involved in steric zippers, which is absent from water-exposed Val residues. This observation indicates that the solvent-exposed Val sidechain undergoes fast rotameric jumps around the Cα–Cβ bond (i.e. the χ_1 angle), thus averaging the $C\gamma_1$ and $C\gamma_2$ chemical shifts. In comparison, Val sidechains at the dry steric zipper interfaces

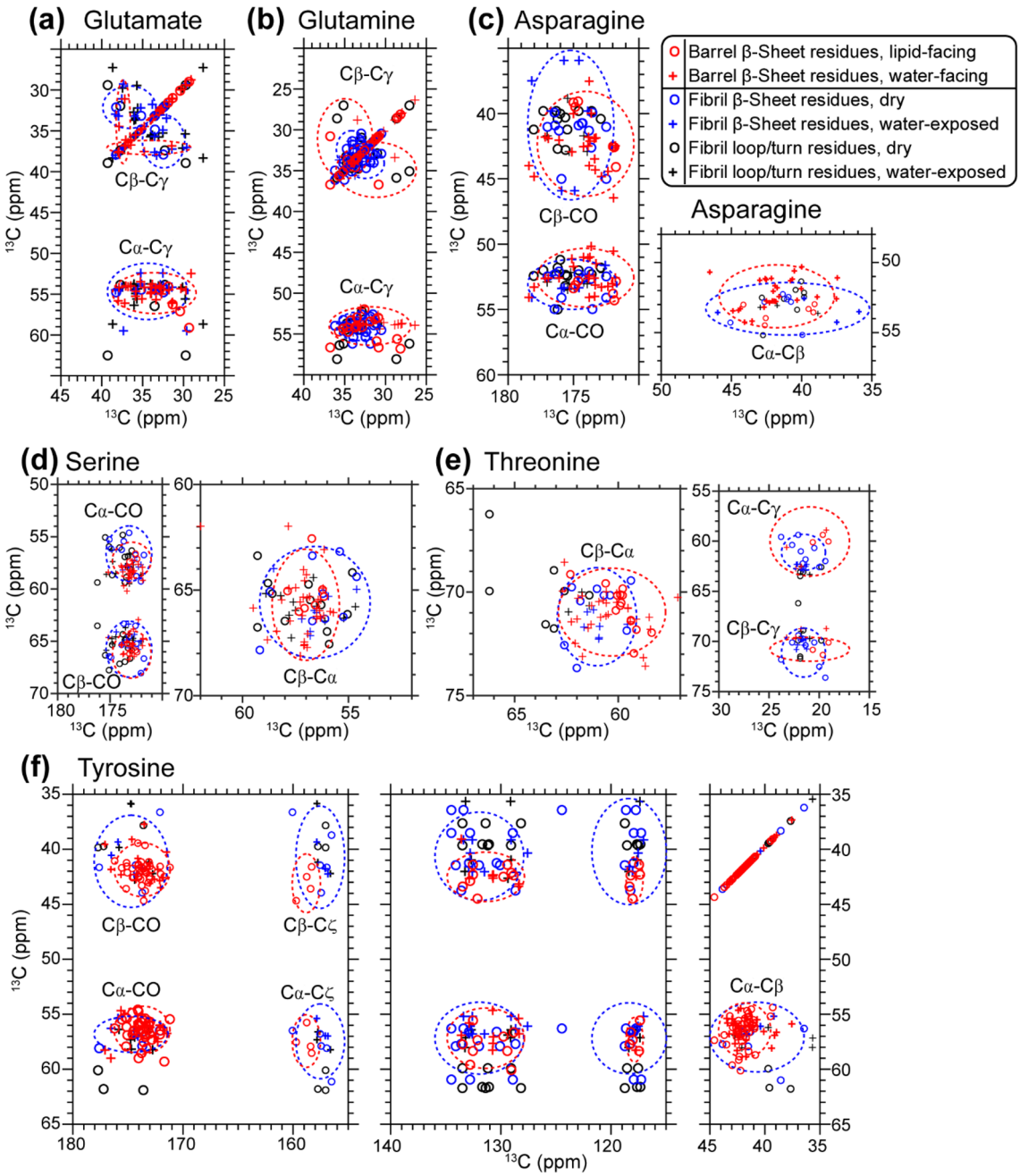

Fig. 7 Selected regions of the 2D ^{13}C–^{13}C correlation maps of polar residues. **a** Glutamate. **b** Glutamine. **C** Asparagine. **d** Serine. **e** Threonine. **f** Tyrosine. Asn and Tyr show a wide distribution of Cβ chemical shifts in fibrils than in β-barrels, while Thr has a narrower Cα chemical shift distribution in fibrils than in β-barrels

are conformationally locked, thus leading to resolved $C\gamma_1$ and $C\gamma_2$ chemical shifts. This effect may also exist for Leu to account for its larger Cδ chemical shift distribution in fibrils than in β-barrels (Fig. 5a). Taken together, Val and Leu sidechains are conformationally more dynamic when they are exposed to either water or lipids as compared to when they reside at β-strand sidechain interfaces.

The conclusion that sidechains involved in steric zippers are more rigid and conformationally distributed than solvent-exposed sidechains is consistent with two studies of amyloid protein dynamics. For HET-s, backbone order parameters were measured using ^{1}H–^{15}N and ^{1}H–^{13}Cα REDOR experiments (Smith et al. 2016). The ^{1}H–^{13}Cα REDOR data show order parameters of 0.8–0.9 for most

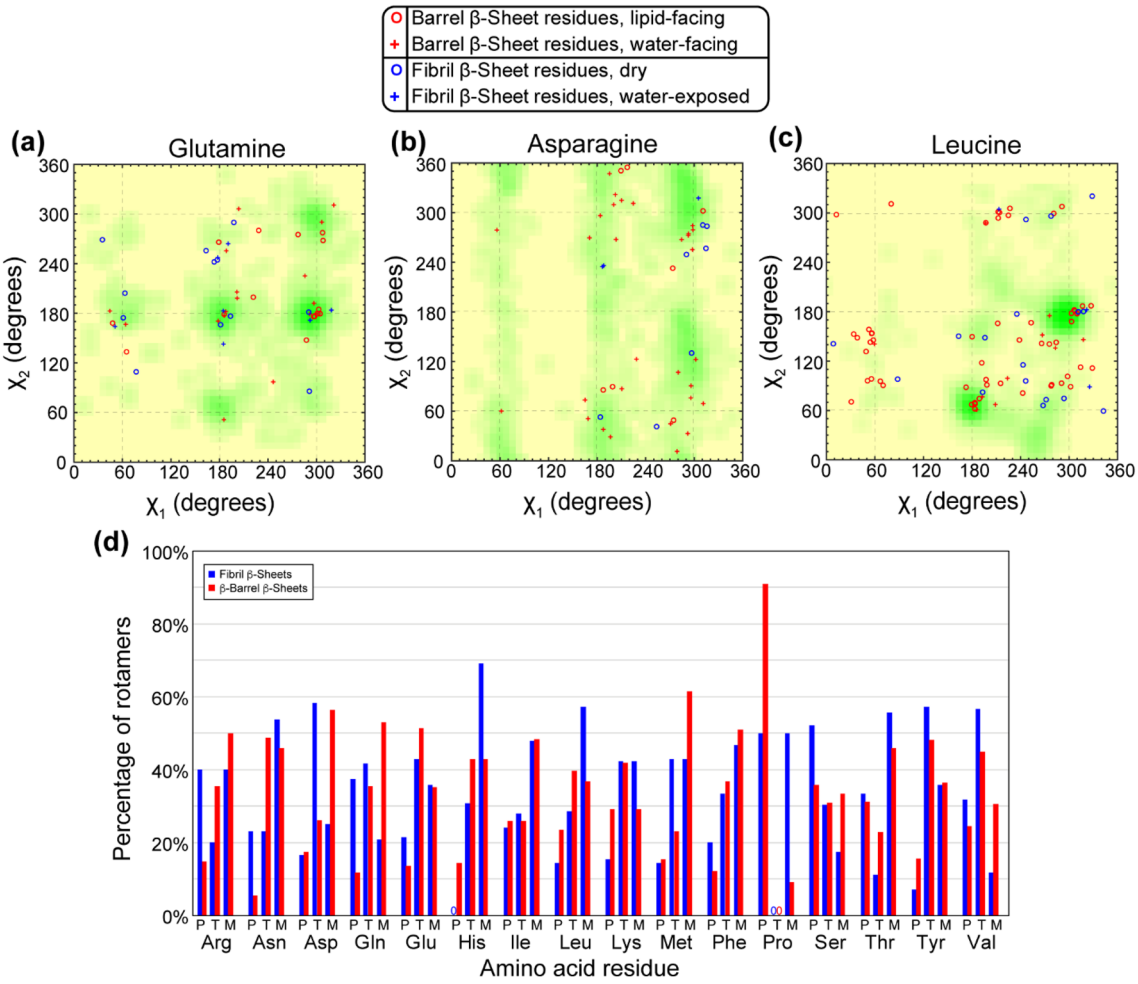

Fig. 8 Sidechain rotamer statistics of amino acids in cross-β fibrils and β-barrel membrane proteins. **a–c** 2D (χ_1, χ_2) angle maps. **a** Glutamine. **b** Asparagine. **c** Leucine (Laskowski et al. 1993, 1996). Green shaded areas indicate the (χ_1, χ_2) distributions found in the PDB, while symbols denote distributions found in the β-sheet proteins examined here. **d** χ_1 rotamer statistics of 16 amino acids in cross-β fibrils (blue) and β-barrel membrane proteins (red). Ala and Gly are omitted due to no χ_1 angle, while Trp and Cys are omitted due to insufficient statistics. χ_1 angles are grouped to one of three states: P (plus, + 60°), T (trans, 180°) and M (minus, -60°). Red or blue zeros (0) indicate that no amino acids occupy that state. For each amino acid, the three bars in each color sum to 100%

solvent-exposed β-strand residues but higher order parameters of 0.9–1.0 for most residues at the dry β-strand interface. This result is consistent with the chemical shift distribution found here. In comparison, the backbone N–H order parameters of β-sheet residues are similarly high, above 0.9. This can be attributed to the fact that the N–H dipolar couplings are dominated by hydrogen bonding along the fibril axis. Another study reported ^{1}H–^{13}Cα order parameters of Aβ40 fibrils (Scheidt et al. 2012) but did not detect a difference between dry and solvent-exposed residues. We tentatively attribute this finding to the packing of multiple protofilaments within the mature fibrils, which may partly immobilize the solvent-exposed β-sheet residues.

Conclusion

This survey of the chemical shifts of more than 2100 residues in amyloid proteins and β-barrel membrane proteins reveal several interesting conformational trends. We found that methyl-rich non-polar residues, polar residues containing sidechain amide and hydroxyl groups, aromatic residues, and small residues, exhibit chemical shift distributions and hence static conformational distributions that are distinct between amyloid fibrils and β-barrels. These chemical shift differences can be explained by sidechain hydrogen-bonding among Gln and Asn residues, van der Waals interactions between methyl-rich Val, Leu and Ile residues in cross-β fibrils, and water or lipid exposure in both types of proteins.

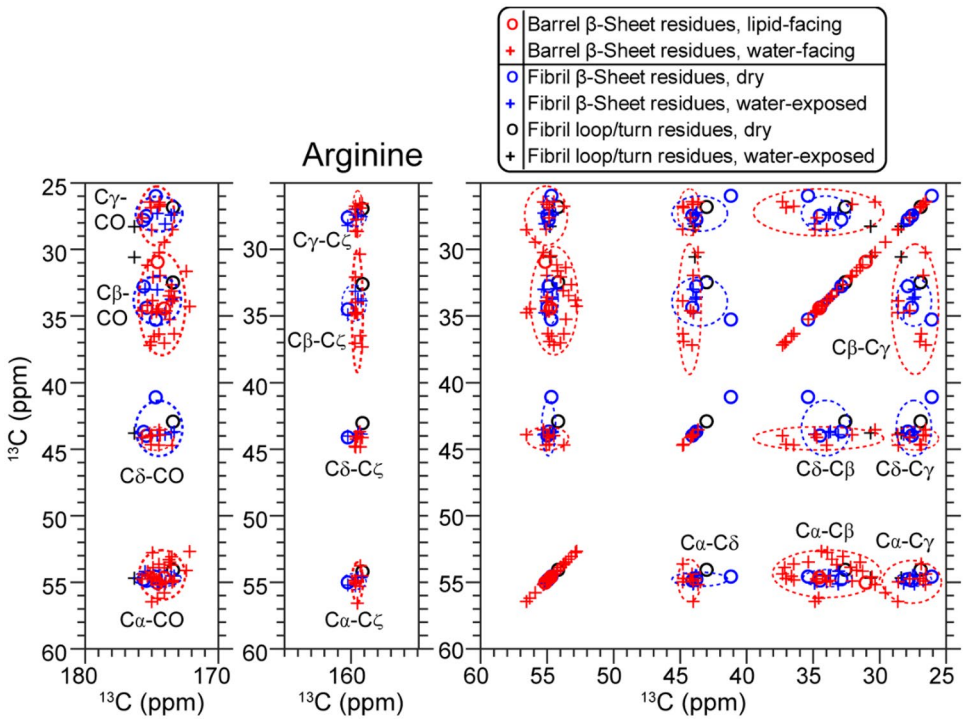

Fig. 9 2D ^{13}C–^{13}C correlation map of arginine. Arg exhibits narrower chemical shift distributions in fibrils than in β-barrels for Cα, Cβ, and Cγ. But for Cδ and Cζ, the β-barrel Arg residues display a narrower chemical shift distribution than fibril residues

These chemical shift trends should be useful for guiding structural analysis of amino acid residues in these β-sheet proteins based predominantly on NMR chemical shifts.

Acknowledgements This work is supported by NIH Grant AG059661 to M.H. and an NIH Ruth L. Kirschstein Individual National Research Service Award (1F31AI133989) to M.D.G.

Data availability The complete chemical shift datasets analyzed in the current study are available from Mei Hong at meihong@mit.edu upon request.

References

Andreas LB et al (2016) Structure of fully protonated proteins by proton-detected magic-angle spinning NMR. Proc Natl Acad Sci USA 113:9187–9192

Bertini I, Gonnelli L, Luchinat C, Mao J, Nesi A (2011) A new structural model of Aβ40 fibrils. J Am Chem Soc 133:16013–16022

Colvin MT et al (2016) Atomic resolution structure of monomorphic Aβ42 amyloid fibrils. J Am Chem Soc 138:9663–9674

Consortium TU (2018) UniProt: a worldwide hub of protein knowledge. Nucleic Acids Res 47:D506–D515

Dregni AJ et al (2019) In vitro 0N4R tau fibrils contain a monomorphic β-sheet core enclosed by dynamically heterogeneous fuzzy coat segments. Proc Natl Acad Sci 116:16357

Dutta SK, Yao Y, Marassi FM (2017) Structural insights into the *Yersinia pestis* outer membrane protein ail in lipid bilayers. J Phys Chem B 121:7561–7570

Edrington TC, Kintz E, Goldberg JB, Tamm LK (2011) Structural basis for the interaction of lipopolysaccharide with outer membrane protein H (OprH) from Pseudomonas aeruginosa. J Biol Chem 286:39211–39223

Fitzpatrick AWP et al (2013) Atomic structure and hierarchical assembly of a cross-β amyloid fibril. Proc Natl Acad Sci 110:5468–5473

Gelenter MD et al (2019) The peptide hormone glucagon forms amyloid fibrils with two coexisting β-strand conformations. Nat Struct Mol Biol 26:592–598

Gremer L et al (2017) Fibril structure of amyloid-β(1–42) by cryo–electron microscopy. Science 358:116–119

Hagn F, Etzkorn M, Raschle T, Wagner G (2013) Optimized phospholipid bilayer nanodiscs facilitate high-resolution structure determination of membrane proteins. J Am Chem Soc 135:1919–1925

Han B, Liu Y, Ginzinger SW, Wishart DS (2011) SHIFTX2: significantly improved protein chemical shift prediction. J Biomol NMR 50:43

Hiller S, Garces RG, Malia TJ, Orekhov VY, Colombini M, Wagner G (2008) Solution structure of the integral human membrane protein VDAC-1 in detergent micelles. Science 321:1206–1210

Horst R, Stanczak P, Wüthrich K (2014) NMR polypeptide backbone conformation of the *E. coli* outer membrane protein W. Structure 22:1204–1209

Johansson MU, Alioth S, Hu K, Walser R, Koebnik R, Pervushin K (2007) A minimal transmembrane beta-barrel platform protein studied by nuclear magnetic resonance. Biochemistry 46:1128–1140

Laskowski R, Macarthur MW, Moss DS, Thornton J (1993) PROCHECK: a program to check the stereochemical quality of protein structures. J App Cryst 26:283–291

Laskowski RA, Rullmannn JA, MacArthur MW, Kaptein R, Thornton JM (1996) AQUA and PROCHECK-NMR: programs for checking the quality of protein structures solved by NMR. J Biomol NMR 8:477–486

Lee M et al (2017) Zinc-binding structure of a catalytic amyloid from solid-state NMR. Proc Natl Acad Sci 114:6191–6196

Liang B, Tamm LK (2007) Structure of outer membrane protein G by solution NMR spectroscopy. Proc Natl Acad Sci 104:16140–16145

Lovell SC, Word JM, Richardson JS, Richardson DC (2000) The penultimate rotamer library. Proteins 40:389–408

Lu J-X, Qiang W, Yau W-M, Schwieters Charles D, Meredith Stephen C, Tycko R (2013) Molecular structure of β-amyloid fibrils in Alzheimer's disease brain. Tissue Cell 154:1257–1268

Mompeán M et al (2018) The structure of the necrosome RIPK1-RIPK3 core, a human hetero-amyloid signaling complex. Cell 173:1244-1253.e1210

Moon CP, Fleming KG (2011) Side-chain hydrophobicity scale derived from transmembrane protein folding into lipid bilayers. Proc Natl Acad Sci USA 108:10174–10177

Morcombe CR, Zilm KW (2003) Chemical shift referencing in MAS solid state NMR. J Magn Reson 162:479–486

Murray DT, Kato M, Lin Y, Thurber KR, Hung I, McKnight SL, Tycko R (2017) Structure of FUS protein fibrils and its relevance to self-assembly and phase separation of low-complexity domains. Cell 171:615-627.e616

Nagy-Smith K, Moore E, Schneider J, Tycko R (2015) Molecular structure of monomorphic peptide fibrils within a kinetically trapped hydrogel network. Proc Natl Acad Sci 112:9816–9821

Nelson R, Sawaya MR, Balbirnie M, Madsen AØ, Riekel C, Grothe R, Eisenberg D (2005) Structure of the cross-β spine of amyloid-like fibrils. Nature 435:773

Paravastu AK, Leapman RD, Yau W-M, Tycko R (2008) Molecular structural basis for polymorphism in Alzheimer's β-amyloid fibrils. Proc Natl Acad Sci 105:18349–18354

Retel JS et al (2017) Structure of outer membrane protein G in lipid bilayers. Nat Commun 8:2073

Sawaya MR et al (2007) Atomic structures of amyloid cross-beta spines reveal varied steric zippers. Nature 447:453–457

Scheidt HA, Morgado I, Rothemund S, Huster D (2012) Dynamics of amyloid β fibrils revealed by solid-state NMR. J Biol Chem 287:2017–2021

Schütz AK et al (2015) Atomic-resolution three-dimensional structure of amyloid β fibrils bearing the osaka mutation. Angew Chem Int Ed 54:331–335

Sgourakis NG, Yau WM, Qiang W (2015) Modeling an in-register, parallel "iowa" aβ fibril structure using solid-state NMR data from labeled samples with rosetta. Structure 23:216–227

Shahid SA, Bardiaux B, Franks WT, Krabben L, Habeck M, van Rossum BJ, Linke D (2012) Membrane-protein structure determination by solid-state NMR spectroscopy of microcrystals. Nat Methods 9:1212–1217

Shen Y, Bax A (2010) SPARTA+: a modest improvement in empirical NMR chemical shift prediction by means of an artificial neural network. J Biomol NMR 48:13–22

Shen Y, Bax A (2013) Protein backbone and sidechain torsion angles predicted from NMR chemical shifts using artificial neural networks. J Biomol NMR 56:227–241

Shen Y, Delaglio F, Cornilescu G, Bax A (2009) TALOS+: a hybrid method for predicting protein backbone torsion angles from NMR chemical shifts. J Biomol NMR 44:213–223

Shen Y et al (2008) Consistent blind protein structure generation from NMR chemical shift data. Proc Natl Acad Sci USA 105:4685–4690

Skora L, Zweckstetter M (2012) Determination of amyloid core structure using chemical shifts. Protein Sci 21:1948–1953

Smith AA, Testori E, Cadalbert R, Meier BH, Ernst M (2016) Characterization of fibril dynamics on three timescales by solid-state NMR. J Biomol NMR 65:171–191

Spera S, Bax A (1991) Empirical correlation between protein backbone conformation and Ca and Cb ^{13}C nuclear magnetic resonance chemical shifts. J Am Chem Soc 113:5490–5492

Su Y, Doherty T, Waring AJ, Ruchala P, Hong M (2009) Roles of arginine and lysine residues in the translocation of a cell-penetrating peptide from (13)C, (31)P, and (19)F solid-state NMR. Biochemistry 48:4587–4595

Tang M, Waring AJ, Hong M (2007) Phosphate-mediated arginine insertion into lipid membranes and pore formation by a cationic membrane peptide from solid-state NMR. J Am Chem Soc 129:11438–11446

Tuttle MD et al (2016) Solid-state NMR structure of a pathogenic fibril of full-length human α-synuclein. Nat Struct Mol Biol 23:409

Ulrich EL et al (2008) BioMagResBank. Nucleic Acids Res 36:D402-408

van der Wel PCA, Lewandowski JR, Griffin RG (2007) Solid-state NMR study of amyloid nanocrystals and fibrils formed by the peptide GNNQQNY from yeast prion protein Sup35p. J Am Chem Soc 129:5117–5130

Vranken WF, Rieping W (2009) Relationship between chemical shift value and accessible surface area for all amino acid atoms. BMC Struct Biol 9:20

Wälti MA et al (2016) Atomic-resolution structure of a disease-relevant Aβ(1–42) amyloid fibril. Proc Natl Acad Sci 113:E4976–E4984

Wasmer C, Lange A, Van Melckebeke H, Siemer AB, Riek R, Meier BH (2008) Amyloid fibrils of the HET-s(218–289) prion form a beta solenoid with a triangular hydrophobic core. Science 319:1523–1526

Wishart DS, Sykes BD (1994) The ^{13}C chemical-shift index: a simple method for the identification of protein secondary structure using ^{13}C chemical-shift data. J Biomol NMR 4:171–180

Wishart DS, Sykes BD, Richards FM (1991) Relationship between nuclear magnetic resonance chemical shift and protein secondary structure. J Mol Biol 222:311–333

Wishart DS, Sykes BD, Richards FM (1992) The chemical shift index: a fast and simple method for the assignment of protein secondary structure through NMR spectroscopy. Biochemistry 31:1647–1651

Wishart DS et al (1995) 1H, 13C, and 15N chemical shift referencing in biomolecular NMR. J Biomol NMR 6:135–140

Xiao Y et al (2015) Aβ(1–42) fibril structure illuminates self-recognition and replication of amyloid in Alzheimer's disease. Nat Struct Mol Biol 22:499